Available online at www.sciencedirect.com
SCIENCE DIRECT®
Computers & Fluids 33 (2004) 869–880
computers & fluids
www.elsevier.com/locate/compfluid

Numerical study of 2D heat transfer in a scraped surface heat exchanger

K.-H. Sun [a,*], D.L. Pyle [a], A.D. Fitt [b], C.P. Please [b], M.J. Baines [c], N. Hall-Taylor [d]

[a] School of Food Biosciences, University of Reading, P.O. Box 226, Reading RG6 6AP, UK
[b] Faculty of Mathematical Studies, University of Southampton, SO17 1BJ, UK
[c] Department of Mathematics, University of Reading, RG6 6AP, UK
[d] Chemtech International Ltd., Reading, RG2 0LP, UK

Received 23 July 2002; received in revised form 10 April 2003; accepted 6 June 2003

Abstract

A numerical study of fluid mechanics and heat transfer in a scraped surface heat exchanger with non-Newtonian power law fluids is undertaken. Numerical results are generated for 2D steady-state conditions using finite element methods. The effect of blade design and material properties, and especially the independent effects of shear thinning and heat thinning on the flow and heat transfer, are studied. The results show that the gaps at the root of the blades, where the blades are connected to the inner cylinder, remove the stagnation points, reduce the net force on the blades and shift the location of the central stagnation point. The shear thinning property of the fluid reduces the local viscous dissipation close to the singularity corners, i.e. near the tip of the blades, and as a result the local fluid temperature is regulated. The heat thinning effect is greatest for Newtonian fluids where the viscous dissipation and the local temperature are highest at the tip of the blades. Where comparison is possible, very good agreement is found between the numerical results and the available data. Aspects of scraped surface heat exchanger design are assessed in the light of the results.

1. Introduction

Scraped surface heat exchangers (SSHEs) are widely used in the food industry for sterilising or cooling highly viscous fluids such as mayonnaise, cream cheese, peanut butter and ice cream. Such

* Corresponding author. Tel.: +44-1183788700; fax: +44-1189310080.
E-mail address: k.sun@reading.ac.uk (K.-H. Sun).

0045-7930/$ - see front matter © 2003 Elsevier Ltd. All rights reserved.
doi:10.1016/j.compfluid.2003.06.009

Nomenclature

$c_1 c_2$	constants
c_m	consistency index (Pa s^m)
C_p	specific heat at constant pressure (J/kg K)
b	heat thinning index $(°C)^{-1}$
h	heat transfer coefficient (W/m^2 s)
I_2	second invariant of the rate of deformation tensor (s^{-1})
k	thermal conductivity (W/m K)
m	shear thinning index (–)
n	unit normal (m)
q	heat flux (W/m^2)
U	inner cylinder speed (m/s)
p	pressure (N/m^2)
Pen	penalty parameter (–)
r	radial location (m)
R_o	inner cylinder radius (m)
R_m	outer cylinder radius (m)
S_V, S_T	convergence constant (–)
T	temperature (°C)
T_o	reference temperature (°C)
T_w	outer cylinder temperature (°C)
ΔT	temperature difference (°C)
$\mathbf{v}$	velocity vector (m/s)
u, v	velocity components (m/s)
V_{max}	maximum velocity component (m/s)
x, y	Cartesian coordinates (m)
$\dot{\boldsymbol{\gamma}}$	rate of deformation tensor (s^{-1})
μ	absolute viscosity ($N\,m/s^2$)
μ_F	characteristic viscosity ($N\,m/s^2$)
ρ	density (kg/m^3)
ω	angular velocity (rad/s)
Re	Reynolds number $Re = \dfrac{\rho U R_o}{\mu_F}$
Pr	Prandtl number $Pr = \dfrac{c_p \mu_F}{k}$
Pe	Peclet number $Pe = \dfrac{\rho c_p U R_o}{k}$
Br	Brinkman number $Br = \dfrac{\mu_F U^2}{k \Delta T}$
Nu	Nusselt number $Nu = \dfrac{h R_m}{k}$

Superscript

*	dimensionless quantity

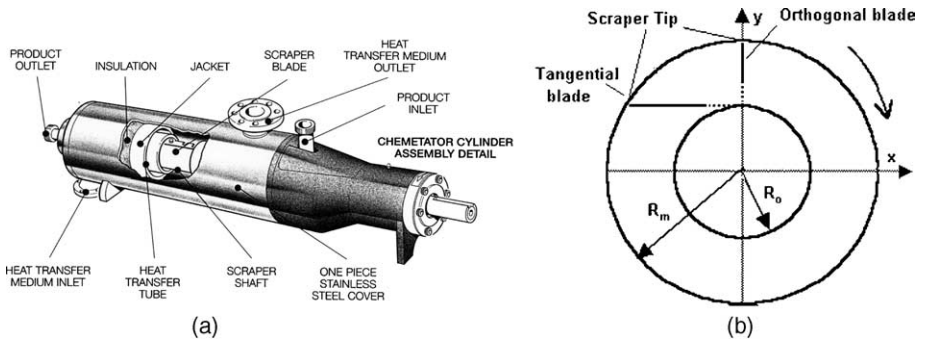

Fig. 1. (a) Expanded view of a scraped surface heat exchanger and (b) schematic view of the 2D cross section studied.

fluids are often non-Newtonian and frequently shear–thin; SSHE operation is a combined thermal and mechanical process whose design and operating principles are poorly understood. In a typical SSHE (Fig. 1a), fluid is slowly pumped along the annulus between a stationary heated or cooled outer cylinder and a rotating inner cylinder. Moving blades attached to the inner cylinder scrape the outer cylinder surface periodically to prevent film formation and promote mixing and heat transfer. The blades are often manufactured with holes or gaps to allow mass flow through the scrapers and to reduce the power required for rotation. In comparison with the axial flow, the rotational flow dominates the mixing process. The high shear region close to the tips of the blades and the significant thermal effects due to viscous dissipation imply that it is crucial to understand the local shear and thermal effects in order to predict heat transfer performance. For highly viscous food materials, thermal diffusion is often very slow compared to convection so that heat becomes trapped inside closed streamlines. It is therefore also of interest to examine how the design and material properties will change the streamlines and stagnation zones in the flow.

Though many SSHE experiments have been carried out, difficulties have been encountered when trying to gain an insight into the interactions between convective and viscous heating. Published experimental SSHE studies were reviewed by Harrod [1]. Analytical studies of certain simplified models for SSHEs have also been reported. For example, Fitt and Please [2] studied the 3D isothermal flow of a power law fluid by applying lubrication theory to small annular-gap/perimeter ratio SSHEs. Their asymptotic analysis provided useful information on velocity profiles and the location of the centre stagnation point between the blades. Also, the optimal energy distribution between rotating and pumping was discussed.

As far as numerical studies are concerned, the fact that the viscosity of many foods is a strong function of both the local shear rate and the temperature, giving a set of highly non-linear governing equations, often causes practical difficulties. Further complications may be introduced by the singularity at the tip of the blades where they scrape the outer cylinder. Martin [3] carried out an early numerical study on heat transfer with power law fluids in a similar geometry. Finite difference approximations were used to study the heating of thermo-plastic melts during screw driven extrusion. The inertia terms were neglected in the momentum equation and the flow was assumed to be fully developed in the axial direction. The temperature distribution was found to be strongly dependent on the thermal boundary conditions that were specified. Finite element techniques were employed by Sun et al. [4] to model forced convection heat transfer with viscous dissipation in steady-state 2D lid driven cavities using power law fluids. The cavity was either

rectangular or diamond shaped (45 degree parallelepiped) and different cavity aspect ratios were considered. A range of thermal boundary conditions was also studied. The results showed that the shear thinning and heat thinning properties of the fluid acted to regulate the local temperature at corners where singularities were present. The results also indicated that gaps in the cavity wall tended to remove the large stagnation area close to the bottom of the downstream wall and thus to improve heat transfer, an effect that was especially pronounced for angled cavities.

For this study, numerical finite element methods were employed using a commercial package Fastflo™ [5] which rather than being a black box CFD code is essentially a finite element partial differential equation solver. The package is designed such that the user can define the problem, set the boundary conditions and control the mesh generation and select appropriate numerical methods and implement these to reach a solution. A Pentium PC with 256 MB RAM and 1 GHz CPU is used for the computation. A series of numerical tests was carried out to ensure numerical stability and solution convergence in both lid driven cavity flow [4] and the current geometry studied. The numerical results were also tested against available published data. Steady-state 2D flow was studied with both closed and cutaway blades (i.e. with a gap for leakage between the blades and inner cylinder) with orthogonal or tangential mounting positions. A modified power law fluid model was used with power law indices of 1.0, 0.8, 0.6 and 0.33. One of the major goals of this study was to assess the independent effects of shear thinning and heat thinning of the material on the local and average heat transfer.

2. Differential equations and numerical procedure

2.1. Governing equations

In an SSHE such as that shown in Fig. 1a, a stationary outer cylinder of radius R_m is maintained at a constant temperature T_w. The blades are attached to the inner cylinder (radius R_o) that rotates at a constant speed U. We assume that the density ρ, thermal conductivity k and specific heat C_p of the fluid being processed are temperature independent and that there is no phase change during device operation. During industrial operation, the mean axial flow speed is much smaller than that of the rotating flow, and in this study the effect of axial flow is neglected. We consider a 2D cross section of the scraped surface heat exchanger in a rectangular coordinate system with the frame of reference attached to the inner cylinder i.e. rotating with angular velocity $\omega = U/R_o$. A schematic view of the cross section studied, the blades mounting positions and the coordinate system is given in Fig. 1b, which shows the outer cylinder rotating in the clockwise direction. For each mounting configuration, four of these blades are evenly spaced around the cylinder circumference.

For incompressible viscous fluids, with the Coriolis force neglected, the dimensionless Navier–Stokes equations can be expressed as [6]

$$\nabla^* \cdot \mathbf{v}^* = 0$$

$$Re\,\mathbf{v}^* \cdot \nabla^* \mathbf{v}^* = -\nabla^* p^* + \nabla^* \cdot \left[\frac{\mu}{\mu_F}\right] \nabla \mathbf{v}^*$$

$$Pe\,\mathbf{v}^* \cdot \nabla^* T^* = \nabla^{*2} T^* + Br\left[\frac{\mu}{\mu_F}\right] I_2^*$$

where $*$ represents a non-dimensional quantity, $\mathbf{v}$, p and T are the velocity vector, pressure and temperature respectively and $I_2 = \frac{1}{2}(\dot{\boldsymbol{\gamma}} : \dot{\boldsymbol{\gamma}})$ is the second invariant of the rate of deformation tensor $\dot{\boldsymbol{\gamma}}$. The characteristic viscosity μ_F is the viscosity evaluated at $\dot{\boldsymbol{\gamma}} = U/R_o$ and a characteristic temperature T_o. The non-dimensional scales for length, velocity and pressure are R_o, U and $\mu_F U/R_o$. The non-dimensional temperature is defined as $(T - T_w)/\Delta T$ and, unless otherwise specified, we shall use $\Delta T = 20$ °C.

The fluid viscosity is both temperature and shear dependent. In this study we used a generalized shear thinning power law expression of the form [6]

$$\mu = c_m e^{-b(T-T_0)} I_2^{(m-1)/2}$$

where c_m is the consistency index, the quantities m and b are the shear thinning and heat thinning indices respectively; both may vary widely with material. A typical value of m for food materials is 0.33 while $m = 1$ corresponds to a Newtonian fluid. The modified non-dimensional expression is

$$\frac{\mu}{\mu_F} = e^{-bT}\left((I_2^* + c_1)^{(m-1)/2} + c_2\right)$$

$$I_2^* = 2\left[\frac{\partial u^*}{\partial x^*}\right]^2 + 2\left[\frac{\partial v^*}{\partial y^*}\right]^2 + \left[\frac{\partial u^*}{\partial y^*} + \frac{\partial v^*}{\partial x^*}\right]^2$$

where the constants c_1 and c_2 are added to ensure that the viscosity has a non-zero finite value in the whole domain. Values of $c_1 = 0.000001$ and $c_2 = 0.0001$ were used. Numerical experiments show that this modification has an insignificant effect on the bulk viscosity and the final numerical results and that it improves convergence.

2.2. Physical parameters and boundary conditions

In the computations reported below, the physical parameters were adapted from data provided by Chemtech International Ltd. The radii of the inner and outer cylinders were 0.05 and 0.075 m respectively, giving a radius ratio of 1.5. For an SSHE with four scrapers, this gives an aspect (length to height) ratio for a typical zone between two scrapers of 3.925. The outer cylinder temperature T_w was set to 0 °C and it was assumed that there was no heat flow across the inner cylinder and the blades. The density, characteristic viscosity and thermal conductivity were taken to be 1200 kg/m^3, 6 N/m s^2 and 0.6 W/m K respectively. The inner cylinder speed was 1 m/s. This gave a Reynolds number $Re = 10$ and a Brinkman number $Br = 0.5$. The non-dimensional numbers will change with changes in parameters such as the characteristic viscosity or rotational speed. For the 2D steady case studied here, it was assumed that there was no axial flow i.e. no net mass flow out of the system. Heat convection occurring inside the system therefore makes no contribution to the total heat transfer. The Nusselt number $Nu = hR_m/k$ where h is the heat transfer coefficient (= heat flux (q)/temperature driving force); thus $Nu = qR_m/k\Delta T = -\mathrm{d}T^*/\mathrm{d}n^*$

where n^* is the unit normal to the surface. Here the total heat flux (or Nusselt number) is independent of Prandtl number: this was verified by the numerical experiments. During the computations a low Prandtl number was used to give a Peclet number $Pe = 100$.

The velocity and thermal boundary conditions were set as

Along the outer cylinder

$$u^* = \frac{R_m}{R_o} \sin\theta$$

$$v^* = \frac{R_m}{R_o} \cos\theta$$

$$T^* = 0.0$$

Along the inner cylinder and blades

$$u^* = 0$$

$$v^* = 0$$

$$\frac{dT^*}{dn^*} = 0.0$$

2.3. Numerical formulation and solution procedure

The governing set of partial differential equations were solved numerically with Fastflo™ using the augmented Lagrangian method. As cited earlier, this package gives the user the freedom to pose the equations and boundary conditions, and to select and modify suitable computational methods. A more detailed discussion of the numerical formulation and solution procedure can be found in [4].

The solution algorithm can be summarised as follows:

(1) An initial temperature field is assumed.
(2) (Inner loop): the temperature dependent viscosity is calculated and the momentum and continuity equations are solved with the given velocity boundary conditions to obtain the pressure and velocity using the augmented Lagrangian method.
(3) Knowing the velocity, the energy equation is solved with the given thermal boundary conditions to update the temperature field.
(4) (Outer loop): steps (2) and (3) are then repeated until both the velocity and temperature fields have converged.

2.4. Convergence criteria and mesh design

Solutions are assumed to have converged and the iteration stops if successive solutions satisfy

$$\sum \left|\mathbf{v}_n^* - \mathbf{v}_{n-1}^*\right| \Big/ \sum \left|\mathbf{v}_n^*\right| < S_V$$

$$\sum \left|T_n^* - T_{n-1}^*\right| \Big/ \sum |T_n^*| < S_T$$

where, for large power law indices ($m >= 0.4$), $S_V = 0.000001$, $S_T = 0.000001$ and for small power law indices ($m < 0.4$), $S_V = 0.0001$, $S_T = 0.0001$.

When generating the mesh, special care has to be taken at the tip of the blades where a singularity is present. For the current heat transfer computation, the mesh also needs to be concentrated along all the surfaces to capture both thermal and momentum boundary layers. This makes creating sufficient mesh points at the tips (four blades) difficult. A small tip gap (2%) is set between the blades and the outer cylinder to reduce the difficulty in creating an acceptable mesh. The mesh is highly concentrated at the tip of the blades and ensures that there at least 5 mesh points across the tip gap. Mesh configurations were tested by checking the effects of mesh refinement on computed values of the stream function and the Nusselt number. Numerical experiments were carried out by increasing the number of nodes from 3470 to 22,602 to ensure that, at the Reynolds numbers studied, both Newtonian and non-Newtonian results were mesh invariant. The final mesh used was composed of non-structured triangular quadratic elements. The total number of nodes used was 14912 with 6908 six-node triangles. Convergence was achieved within 15 iterations.

2.5. Comparison with analytical solutions in tangential annular flow

An important credibility check was conducted by comparing the numerical results with analytical solutions for tangential annular flow in an annulus without scraper blades. Martin [3] gives a rather involved analytical solution for the tangential annular flow of shear thinning and heat thinning fluids. By neglecting heat thinning, a very simple analytical expression may be obtained which is briefly described as follows. For tangential annular flow between a stationary ($\omega = 0$) inner cylinder of radius R_o and a rotating outer cylinder of radius R_m, assuming an adiabatic inner cylinder and that the outer cylinder is maintained at a constant temperature T_w, the temperature in the annulus can be expressed as

$$T = T_w + Br\left(\frac{2}{m}\right)^{m-1}\left(1 - \left(\frac{R_o}{R_m}\right)^{2/m}\right)^{-m-1}\left(\left(\frac{R_o}{r}\right)^{2/m} - \left(\frac{R_o}{R_m}\right)^{2/m} + \ln\left(\frac{r}{R_m}\right)^{2/m}\right)\Delta T$$

where the Brinkman number is $Br = \dfrac{\mu_F U^2}{k\Delta T} = \dfrac{c_m R_o^2 \omega^{m+1}}{k\Delta T}$.

The average heat flux is thus

$$Nu = \frac{R_o}{\Delta T}\left.\frac{dT}{dr}\right|_{r=R_m} = Br\left(\frac{2}{m}\right)^m \frac{R_o}{R_m}\left(1 - \left(\frac{R_o}{R_m}\right)^{2/m}\right)^{-m}$$

A comparison between analytical and numerical results with $Br = 0.5$ and 1.0 is given in Fig. 2. The difference is within 0.1%. Bearing in mind the modifications made to the power law in the numerical results, this may be regarded as excellent agreement.

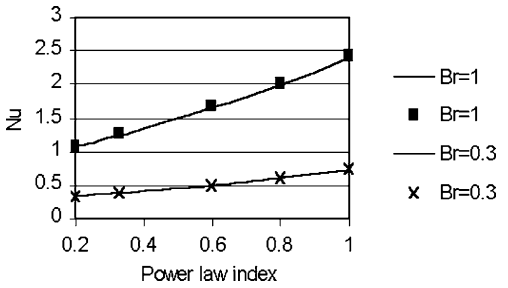

Fig. 2. Nusselt number at the outer cylinder for tangential flow in an annulus. Solid lines—analytical results; symbols—numerical results.

3. Results and discussion

3.1. Effect of blade design on the flow and the heat transfer

Numerical results were calculated for $Re = 10$, $Pr = 10$ and a Brinkman number of 0.5 with a heat thinning index of 0.05 $^{\circ}C^{-1}$ and power law indices of 1, 0.8, 0.6 and 0.33 for different gap sizes at the root of the blades. For each set of conditions, the velocity, pressure and temperature fields were determined. The location of the stagnation point between the blades, the net force acting on each blade and the heat flux at the outer cylinder were then calculated. The results show that for a shear thinning material the velocity profiles on the centre line between two blades are flattened and the location of the centre stagnation point is shifted. Fig. 3 shows the velocity profiles on the centre line between two closed orthogonal blades. The net force reduces with increasing gap size and decreasing shear-thinning index. With 20% gap cutaway blades the net force is reduced by 20% with orthogonal blades and 28% with tangential blades. The gap size also affects the location of the centre stagnation point, the temperature distribution and the heat flux. For $m = 0.33$, the streamlines are given in Fig. 4a (orthogonal blades) and Fig. 4b (tangential blades). Temperature contours for orthogonal blades are given in Fig. 5. In all the contour plots displayed, the contour value varies from 0 at the outer cylinder to its maximum value. We observe that as the gap increases the high temperature region moves from downstream of the blades towards the inner cylinder. With a 60% gap the centre stagnation zone is completely absent, but the hot material close to the inner cylinder is trapped. The average heat flux for different gap sizes and

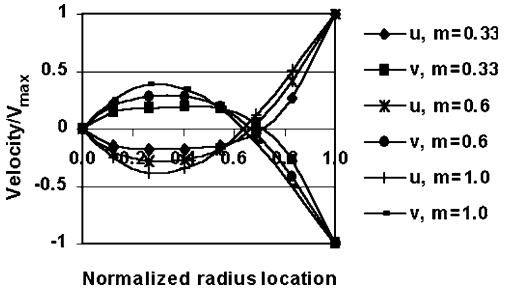

Fig. 3. Effect of shear thinning index on the velocity profiles between two closed orthogonal blades.

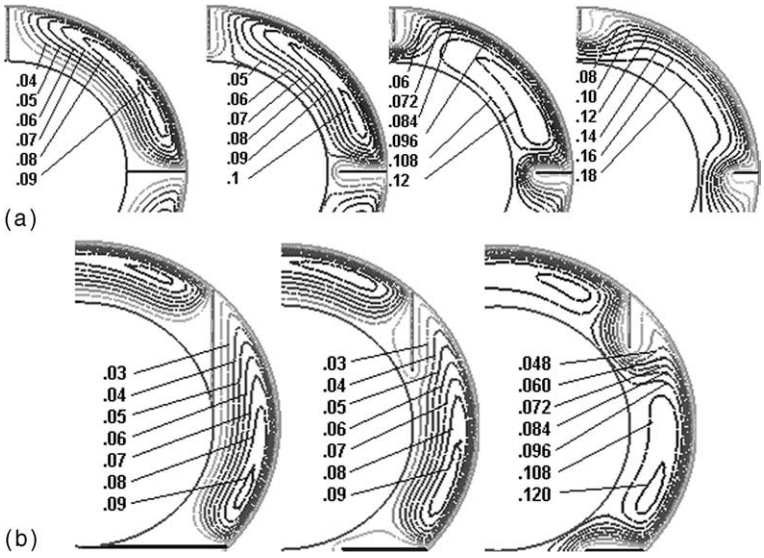

Fig. 4. (a) Effect of gap size on flow streamlines for $m = 0.33$ with orthogonal blade, from left 0%, 20%, 40%, 60% gap. The stream function value at the outer cylinder is 0. (b) Effect of gap size on flow streamlines for $m = 0.33$ with tangential blade, from left 0%, 20%, 40% gap. The stream function value at the outer cylinder is 0.

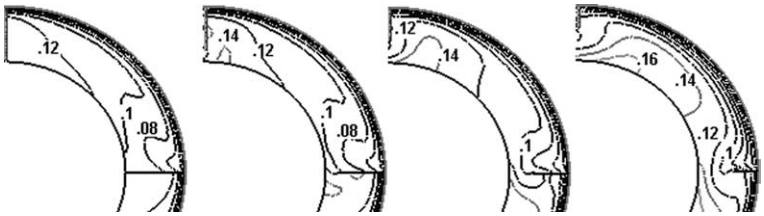

Fig. 5. Effect of gap size on dimensionless temperature contours for $m = 0.33$ with orthogonal blade, from left 0%, 20%, 40%, 60% gap. The contour value at the outer cylinder is 0.

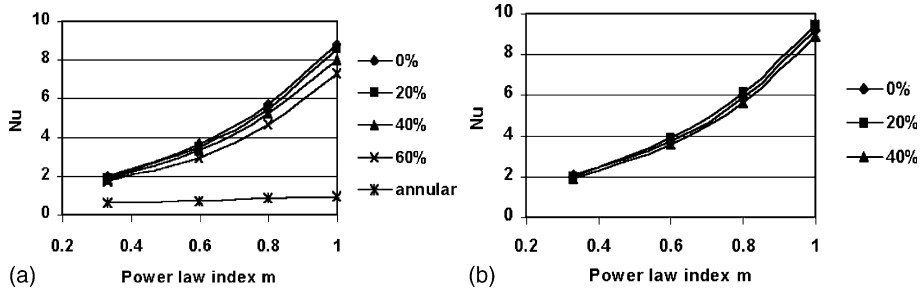

Fig. 6. Effect of gap size on averaged heat flux (a) orthogonal blades and (b) tangential blades.

blade mounting positions is shown in Fig. 6a and 6b. With orthogonal blades, the average heat flux is reduced by less than 3% for a 20% gap. For tangential blades, however, the heat flux is

increased by 3% for a 20% gap. This may be explained by the removal of the large stagnation zone upstream of the tangential blades (see Fig. 4b).

3.2. The effects of shear thinning and heat thinning on heat transfer

To study the effects of shear and heat thinning, values of the heat thinning index of 0.0, 0.05 and 0.1 were used. The temperature contours for orthogonal mounted blades with a 20% gap are shown in Fig. 7. We observe that, for the Newtonian case, the highest temperatures are found close to the singularity corners. As the power law index decreases the high temperature zone moves away from the singularity corners. We also note that, for shear thinning and heat thinning fluids, viscous dissipation is reduced close to the singularity corner. As a result, the local heat fluxes and also the average heat fluxes are reduced. This can be seen in Fig. 8a and 8b. The normalized distance is the location of the points along the outer cylinder projected onto the x coordinate and divided by the radius of the outer cylinder. The lower the shear thinning index, the lower the local viscous dissipation and heat flux near the singularity corner. This may be understood as ''self-adjustment'' of the power law fluid close to the singularity corners. The heat thinning effect is most significant for Newtonian fluids where viscous dissipation and the local temperature are maximised at the tips of the blades. It is the local high temperature that brings the heat-thinning factor into play. The influence of m and b depends upon combinations of the relevant non-dimensional parameters and also on the fluid temperature. The results are consistent with the results found for cavity flow by Sun et al. [4].

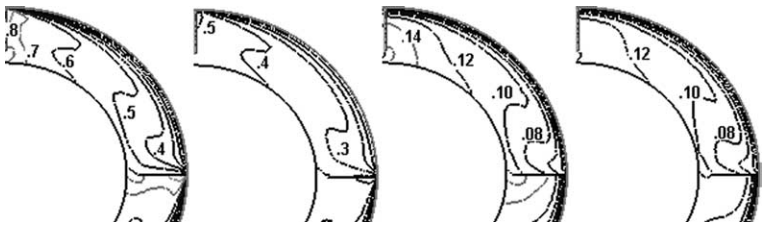

Fig. 7. The effect of m and b on dimensionless temperature contours (20% gap; orthogonal blades). From left $m = 1$, $b = 0$; $m = 1$, $b = 0.1$; $m = 0.33$, $b = 0$; $m = 0.33$, $b = 0.1$. The contour value at the outer cylinder is 0.

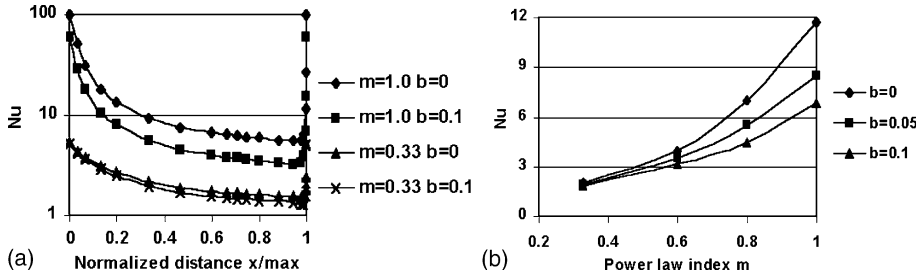

Fig. 8. Heat flux at outer cylinder for 20% gap orthogonal blade. (a) Local heat flux and (b) averaged heat flux.

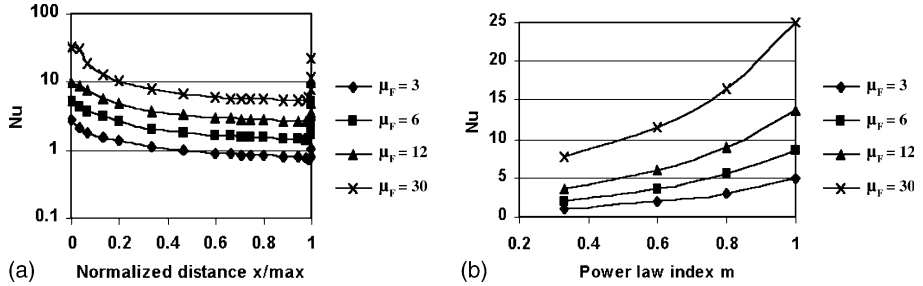

Fig. 9. Effect of characteristic viscosity on heat flux for 20% gap orthogonal blade. (a) Local heat flux for $m = 0.33$ and (b) averaged heat flux.

3.3. The effects of characteristic viscosity on heat transfer

For practical SSHE operations, frequently the characteristic viscosity is the only parameter that changes between production runs. Using conditions otherwise identical to those used in Section 3.1, for characteristic viscosities of 3, 6, 12 and 30 N/m s^2, the relevant Reynolds and the Brinkman numbers were $Re = 20$, 10, 5, 2 and $Br = 0.25$, 0.5, 2 and 2.5, respectively. As explained in Section 2.2, Pr will not affect the total heat transfer for the current configurations. To get the same resolution at the wall for the same mesh, the Peclet number remains unchanged. Fig. 9 shows the effect of characteristic viscosity on the Nusselt number at the outer cylinder for a 20% gap orthogonal blade. With a characteristic viscosity of 30 N/m s^2, $Re = 2$ and $Br = 2.5$, a relaxed convergence threshold had to be set for $m > 0.6$ because of the high viscous dissipation involved. We observe that the Nusselt number increases with increasing characteristic viscosity.

4. Conclusions

We have successfully used finite element methods to study forced convection heat transfer in a steady 2D model of scraped surface heat transfer with power law fluids. The numerical results give excellent agreement with analytical results where comparison is possible. For shear thinning materials, the velocity profiles at the centre line between two blades become flattened, the location of the centre stagnation point is shifted and the net force on the blades is reduced. For a constant viscosity fluid, the high shear at the singularity corners gives rise to high viscous heating; the maximum temperature and heat flux are close to the tip of the blades. For shear thinning fluids, the viscosity is reduced in the high shear region so that both the local viscous heating and the local wall heat flux are reduced. The heat thinning acts to reduce the viscosity in the high temperature zone and as a result it also reduces viscous heating and wall heat flux. As the power law index decreases, the location of the maximum temperature moves away from the singularity corners. Its location will depend on the particular combination of the parameters describing the flow.

The gap at the root of a blade acts to remove the stagnation zone in this region, and also reduces the net force on the blades and shifts the location of the centre stagnation point. Small gaps on tangential blades enhance heat transfer by removing the large stagnation area upstream

of the blades. Too large a gap should be avoided, since this appears to cause a reduction in convective mixing and wall heat flux.

The results that have been presented here are two-dimensional only. The heat transfer is thus dominated by viscous dissipation that is mainly created close to the tip of the blades. The heat transfer is greatly affected by the characteristic viscosity and the variation in the local viscosity by shear and heat thinning. Further research is underway to incorporate axial flow into the model.

Acknowledgements

This research is supported by The University of Reading and Chemtech International. The first author acknowledges financial support from The University of Reading.

References

[1] Harrod M. Methods to distinguish between laminar and vortical flow in scraped surface heat exchangers. J Food Proc Eng 1990;13(1):39–59.
[2] Fitt AD, Please CP. Asymptotic analysis of the flow of shear-thinning food stuffs in annular scraped heat exchangers. J Eng Math 2001;39:345–66.
[3] Martin B. Numerical studies of steady state extrusion process. PhD thesis, Cambridge University, 1969.
[4] Sun K-H, Pyle DL, Fit AD, Please CP, Hall-Taylor N, Baines MJ. Numerical modelling of non-Newtonian heat transfer with viscous dissipation in lid driven cavities. AICHE J, submitted for publication.
[5] Fastflo Tutorial Guide V3, Oxford, Numerical Algorithms Group, 2000.
[6] Bird RB, Armstrong RC, Hassager O. Dynamics of polymeric liquids. In: Fluid mechanics, 2nd ed., vol. 1. New York: John Wiley; 1987.